Performance Limitations in Sensorimotor Control: Tradeoffs between Neural Computing and Accuracy in Tracking Fast Movements

Shreya Saxena[1], Sridevi V. Sarma[2] & Munther Dahleh[1]

[1]*Department of Electrical Engineering and Computer Sciences, Massachusetts Institute of Technology, Cambridge MA 02139*

[2]*Department of Biomedical Engineering, Johns Hopkins University, Baltimore MD 21210*

The ability to move fast and accurately track moving objects is fundamentally constrained by the biophysics of neurons and dynamics of the muscles involved. Yet, the corresponding tradeoffs between these factors and tracking motor commands have not been rigorously quantified. We use feedback control principles to identify performance limitations of the sensorimotor control system (SCS) to track fast periodic movements. We show that (i) linear models of the SCS fail to predict known undesirable phenomena, including skipped cycles, overshoot and undershoot, produced when tracking signals in the "fast regime", while nonlinear pulsatile control models can predict such undesirable phenomena, and (ii) tools from nonlinear control theory allow us to characterize fundamental limitations in this fast regime. Using a validated and tractable nonlinear model of the SCS, we derive an analytical upper bound on frequencies that the SCS can reliably track before producing such undesirable phenomena as a function of the neurons' computational complexity and muscle dynamics. The performance limitations derived here have important implications in sensorimotor control.

For example, if primary motor cortex is compromised due to disease or damage, the theory suggests ways to manipulate muscle dynamics by adding the necessary compensatory forces using an assistive neuroprosthetic device to restore motor performance, and more importantly fast and agile movements. Just *how* one should compensate can be informed by our SCS model and the theory developed in this paper.

Tracking fast unpredictable movements is a valuable skill, applicable in many situations. In the animal kingdom, the context includes the action of a predator chasing its prey that is running and dodging at high speeds, for example, a cheetah chasing a gazelle. The sensorimotor control system (SCS) is responsible for such actions and its performance clearly depends on the computing power of neurons and the dynamics of muscles involved. Despite these obvious factors that set the limits on how fast an animal can track a moving object, tracking performance of the SCS and its dependence on neural computing and muscle dynamics has not been explicitly quantified. This study aims to rigorously quantify the performance tradeoffs between accurately tracking fast moving objects, in particular periodic inputs, and the computing power of neurons subject to their biophysical constraints. The tradeoffs are also described as a function of muscle dynamics.

Tracking periodic signals is in itself an experimental paradigm that has been explored in many visuo-motor and memory tasks [1,2]. It has been shown in experimental settings that tracking faster and faster periodic inputs leads to a regime where subjects skip cycles because they are unable to keep up. In [3], monkeys performed an oculomotor task in which they were required to track periodic inputs with their eye muscles. Tracking was shown to be accurate at low frequencies,

but as the frequency of the input increased, the monkeys performance deteriorated and they started to skip cycles (Fig. 1A). In [4], human subjects were asked to make quick periodic downward-upward motions upon hearing a periodic auditory stimulus. As expected, when the frequency of the input increased, accuracy decreased. More importantly, several undesirable phenomena including overshoot, undershoot, and skipped cycles were observed in the high frequency regime (Fig. 1B).

We hypothesize the existence of a fundamental frequency, ω_c, above which we observe these undesirable phenomena when tracking sinusoidal inputs. To test our hypothesis, we set out to (i) construct a mathematical model of the SCS consisting of a feedback interconnection between the cerebrocerebellar system, alpha motor neurons and the musculoskeletal system, and then (ii) develop formal methods to prove the existence of and to compute ω_c as a function of our model parameters.

Although tracking in motor control has been well studied, with competing mathematical models to describe the phenomena observed [1], the applicability of these models in the regime of tracking *high frequency* periodic signals has been overlooked. One possible reason is due to analytical tractability of experimentally validated models. Linear models of the SCS are simple to analyze [5], but they fail to capture the undesirable tracking phenomena observed experimentally. For example, discontinuities appearing in slow movements are a well known feature that have been studied to elucidate the wiring in the downstream alpha motor neurons. Specifically, during slow movements, discontinuities in the finger position have been observed, even when subjects try hard

to follow a smooth trace. These discontinuities are not captured with linear models of the SCS.

Due to these limitations of linear models, the threshold-based pulsatile control of movements was first suggested in 1947 [6], and since then has been in active exploration in the feedback setting [1,7–13]. Here, we construct an analytically tractable model of the SCS that reproduces several characteristics of neuronal and motor outputs in response to periodic inputs in both the slow and fast regimes observed in humans and primates both in health in in disease. In particular, the input, $r(t)$, drives a response, $z(t)$, from a linear model of the cerebrocerebellar system, that in turn generates a control signal, $u(t)$, from a group of alpha motor-neurons. These motor neurons then actuate a linear model of the musculoskeletal system that generates the motor output which is fed back to the brain (see Fig. 2). The critical part of our SCS model that must remain biophysically-based and nonlinear is how *alpha motor neurons* encode signals from the cerebrocerebellar system in the form of spike events.

We then derive conditions for which tracking a sinusoidal input produces undesirable phenomena as a function of the parameters of the closed-loop system. Specifically, we show that for a fixed musculoskeletal system M, cerebrocerebellar dynamics K, and a group of motor neurons with spiking thresholds q (for activation of agonist/antagonist pair of muscles), the oscillatory input (periodic back-and-forth movement) with frequency ω may generate undesired skipped cycles if $\omega > \omega_c(M, K, q)$.

The results derived here make a scientific contribution in advancing our understanding of how movement speeds may be limited given the processing of the driving signal through neurons.

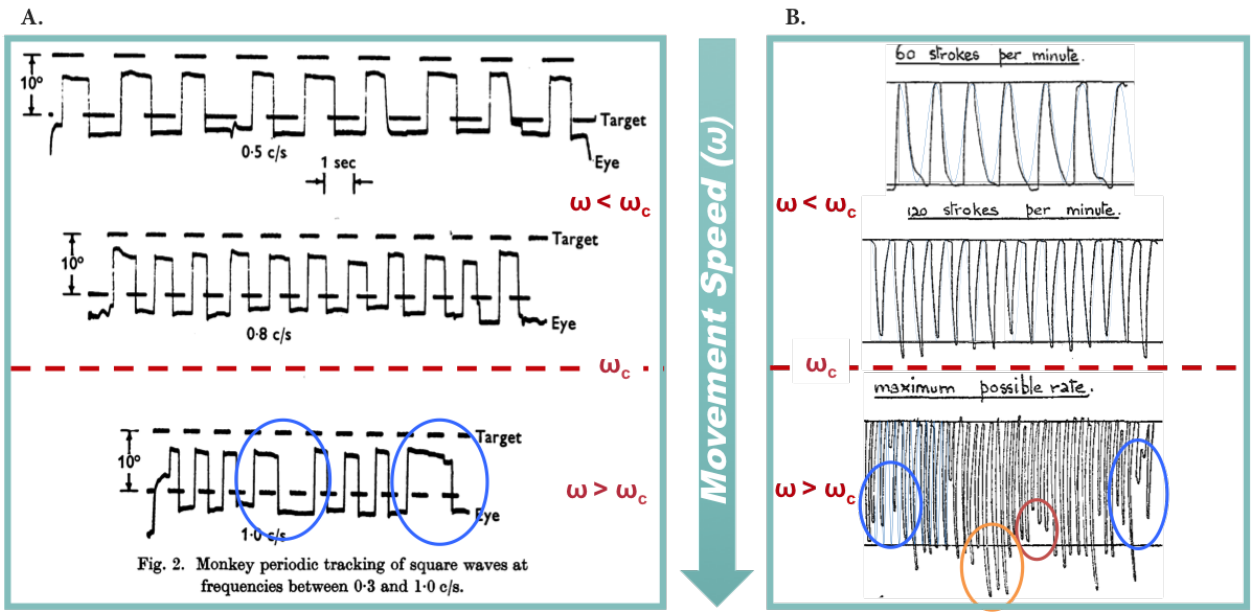

Figure 1: Undesirable phenomena as seen in experiments; A: oculomotor tracking by a non-human primate, adapted from [3], and B: pursuit tracking based on an auditory cue, adapted from [4]. In both cases, fairly accurate tracking is seen in relatively low frequency reference signals (i.e. $\omega < \omega_c$), whereas undesirable phenomena such as skipped cycles (blue circles), overshoot (orange circle) and undershoot (red circles) are seen in high frequency signals for $\omega > \omega_c$ for some ω_c.

The characterization of ω_c for sinusoidal movements provides a theoretical basis for further investigation for more general classes of movements. By providing a concrete dependance on the parameters of the system, our analysis can also guide the design of therapies for movement disorders caused by a compromise in K, q or M.

Model of Sensorimotor Control

Fig. 2 shows a schematic of our SCS model and its components, which are similar to previous models for sensorimotor control [16,19–21]. We assume that the SCS input is the intended voluntary movement or reference signal, $r(t)$, that exists in some part of the brain (e.g. in parietal regions). The reference input is processed by brain structures including the sensorimotor, premotor and motor cortices, and ultimately the neurons in premotor and motor areas send spike train signals to muscles via the spinal cord. Appropriate muscles are innervated to generate a movement, $z(t)$, as the system attempts to follow or "track" $r(t)$. The generated movement (output of SCS) is then fed back, via proprioceptive and visual feedback, represented by a feedback gain F, to be processed by structures including the cerebellum and sensorimotor cortex. There are other structures involved in the generation of movements such as the basal ganglia and motor thalamus not explicitly shown.

We break down our SCS model into two general components: neural dynamics and the musculoskeletal system. The neural dynamics consists of a) cerebrocerebellar processing of the error between intended and actual movement and b) alpha motor neuron encoding of cortical motor

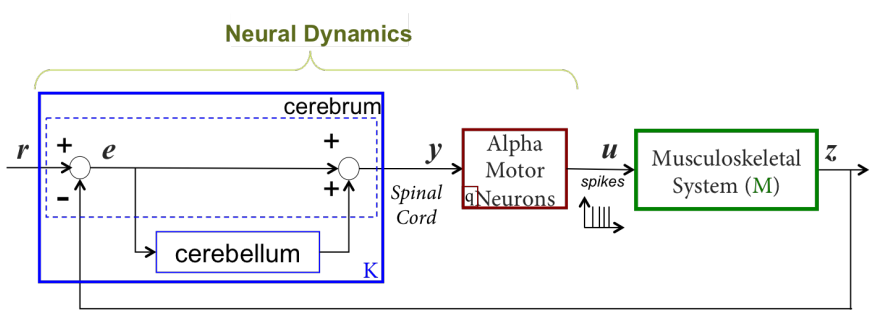

Figure 2: Closed Loop Model at a high level

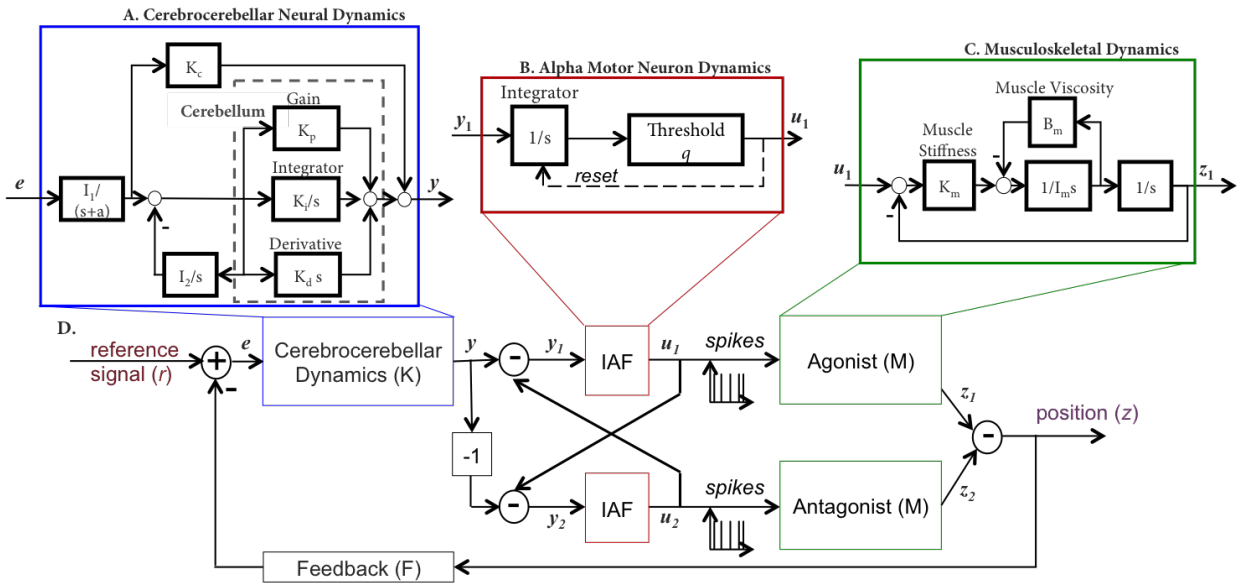

Figure 3: Proposed closed-loop model for movement generation. A. Details of cerebrocerebellar dynamics, adapted from [14–16]. B. Details of the IAF Model [17]. C. Details of the musculoskeletal system, adapted from [18]. D. A closed-loop model of the agonist / antagonist muscles acting around a single joint.

commands. Below, we describe each model component. Importantly, the results derived in the Methods apply for a broad class of cerebrocerebellar as well as musculoskeletal models.

Neural Dynamics We take a systems approach to model neural dynamics. Specifically, we use a previously validated model of cerebrocerebellar processing [16] that describes how motor cortical areas integrate with cerebellar processing of errors between intended and actual kinematics. This model characterizes firing rate activity of populations of cerebellar and cortical neurons during movement, and produces an analog signal that is then sent to an integrate-and-fire (IAF) model describing the spiking responses of groups of alpha motor neurons.

The concept of *neural computing* can be thought of as the density of the resulting spike trains that directly drive muscle activity. The higher the density of the spikes, the more information is flowing from the neural system to the musculoskeletal system. Due to energy and efficiency constraints [22], the nervous system is thought to converse in the language of spikes, which puts a heretofore underdetermined limitation on the ability to track fast movements. We explore this tradeoff in this study, while detailing the models used for the neural and musculoskeletal dynamics below.

A. Cerebrocerebellar Dynamics

A basic cerebrocerebellar system diagram is given in Fig. 3A [14–16]. To begin with an analytically tractable SCS model, we characterize the cerebrocerebellar SCS component as a dynamical feedback control system (K) that compares the intended movement with actual movement. Much available behavioral and neurophysiological data on human and animal cerebellar motor control relates to stabilization of posture and accurate control of movements rather than explicit control of contact force or joint torques. Importantly, though, because of the uniformity of its circuitry, intra-cerebellar mechanisms are almost certainly common to both position and force control systems, especially for fast movements. This motivates our choice of modeling the cerebrocerebellar system, K, as belonging to a class of linear time invariant systems including proportional (K_p), integral (K_i) and derivative (K_d) (PID) controllers as in [16,19–21].

More specifically,

$$K(s) = I_1 \left(\frac{K_c}{s} + \frac{K_{cbl}(s)}{s + I_2} \right) \tag{1}$$

$$K_{cbl}(s) = a_p + \frac{a_I}{s} + a_d s \tag{2}$$

More information about the cerebrocerebellar dynamics is provided in the Supplementary Information.

B. Alpha Motor Neuron Dynamics

Alpha motor neurons are driven by the output of the cerebrocerebellar system and have been described as the "final common pathway" of the motor system by the English physiologist and Nobel Prize winner, Charles Sherrington,[23] because their activity directly drives muscles. Consequently, we maintain the spiking or pulstile nature of alpha motor neuron control of muscles by modeling them with generalized integrate-and-fire (IAF) models, which have been used to model motor neurons in both experimental and computational studies [24,25].

For each joint in our muscle model described in , we characterize an "effective agonist group of motor units" and an "effective antagonist group of motor units". More specifically, we assume that each group of motor units generates spikes in an IAF fashion (see Fig. 3 B). That is, each group integrates the tracking error signal $e(t)$, and after the integral reaches a firing threshold $\pm q$,

it outputs a ‘positive’ or a ‘negative’ spike and resets back to resting potential $v(0)$. Specifically, the voltage across the membrane of neuron i is accumulated over time as:

$$v(t) = \int_0^t e(t) + v(0) \tag{3}$$

When $v(t) > q$, a weighted positive spike, $q\delta(t)$, is produced. If $v(t) < -q$, a weighted negative $-q\delta(t)$, is produced. The collection of positive spikes $u_1(t) = \sum_{i\in\mathcal{R}} q\delta(t - t_i^p)$ is the spike train generated collectively by neurons in the effective agonist group of motor units, and the collection of negative spikes (represented as positive action potentials in brain) $u_2(t) = \sum_{i\in\mathcal{R}}(-q)\delta(t - t_i^n)$ is the spike train generated collectively by neurons in the effective antagonist group of motor units. That is, model (3) generates two spike trains, the positive spikes actuate the agonist muscle by activating an appropriate group of motor units, and the negative spikes actuate the antagonist muscle by activating another group of motor units. The weight of the spike is chosen to be the same as the integral, following the Henneman’s size principle [26]. In general, if we have more than one neuron innervating the muscle, the innervation amplitude should be proportional to the activation threshold in keeping with the Henneman’s size principle.

This abstraction of spinal cord processing is motivated by the fact that several spike trains from the brain (M1 and premotor areas) get transmitted to several alpha motor neurons via the corticospinal tract, which then get processed by an “effective agonist group of motor units” and an “effective antagonist group of motor units”. Recall that the collection of the alpha motor neurons

and the set of fibers it activates is called a "motor unit". These groups in turn innervate extrafusal muscle fibers of skeletal muscle and are directly responsible for initiating their contraction. An increase in 'neural computation' follows an increase in the density of the relevant spike trains, i.e. a decrease in the spiking threshold q.

Musculoskeletal Dynamics We use a single joint model of the musculoskeletal system as in [18] (Fig. 3C), though our methods easily extend to multiple joint systems. The transfer function of this model from the neural activity (u) to the limb output (z) is the following.

$$M(s) = \frac{K_m}{I_m s^2 + B_m s + K_m} \tag{4}$$

As shown in Fig. 3C, K_m corresponds to the net stiffness of all muscles acting around the joint, as determined by the level of agonist/antagonist coactivation, B_m is the net viscosity, and I_m is the inertia. This model is taken from the class of "equilibrium-point models" for motor control [18]. Under this class of models, the mechanical properties of muscles and the myotactic reflexes generate equilibrium positions for the limb. If the limb is displaced from rest position, the spring-like properties of the muscles generate the appropriate restoring torques to return the limb to rest (equilibrium). These models are in reasonable agreement with experimental data, yet are simple enough to analyze. More information about the musculoskeletal model is provided in the Supplementary Information.

Results

In this section, we first demonstrate how our closed-loop SCS model reproduces fundamental properties of alpha motor neuron activity during movement generation and responses to several types of reference signals observed in both healthy subjects and cerebellar patients. Then we derive the fundamental frequency, ω_c as a function of model parameters, and describe its sensitivity to SCS model parameters. Finally, we show how a simple compensator at the musculoskeletal end can restore ω_c in the cerebellar SCS model.

SCS Model Reproduces Observed Phenomena in Health and in Disease Our SCS model displays several important experimental properties that alpha motor neurons are known to have. These properties are shown in Figure 4 which compare data to model simulations. Fig. 4A shows the Henneman's size principle obeyed by alpha motor neurons [27]. The more force that is needed, the more motor units are recruited in a precise order according to the magnitude of their force output, with small units being recruited first. In order to reproduce the Henneman's size principle using our SCS model, we simulated a network of neurons, with the cerebrocerebellar output,y, going into multiple IAF models. The output of this network was a scalar consolidated weighted spike train. The weights on the consolidated spike train corresponded to the integral of y since the last spike from any IAF.

Fig. 4B illustrates how motor neurons may produce plateau potentials, resulting in self-sustained firing, providing a mechanism for translating short-lasting synaptic inputs into long-lasting motor output. This self-sustained oscillatory behavior is a key property observed in more

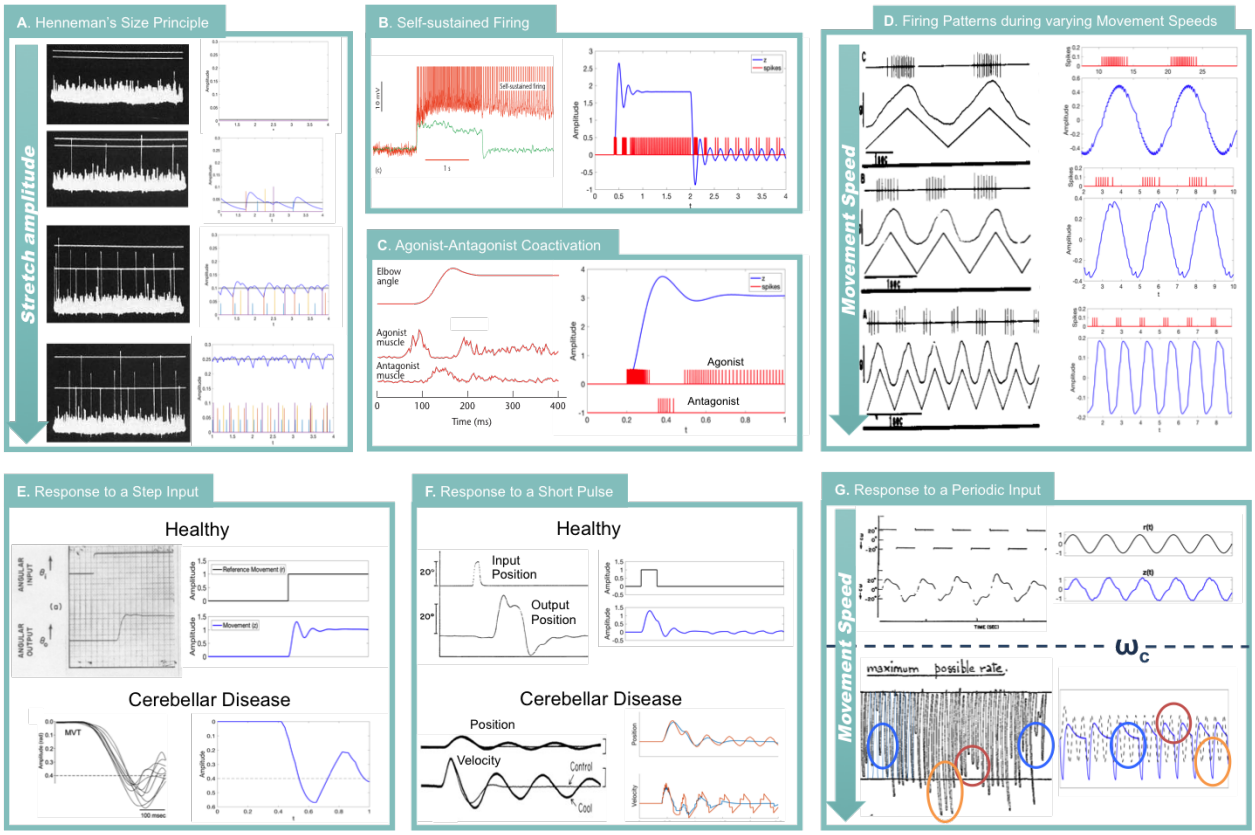

Figure 4: Model reproduces known properties and responses to elemental signals. In all these diagrams, to the left is experimental data from literature, adapted from the sources mentioned, and to the right are simulations using our model. Top Row: Experimental properties displayed in alpha motor neuron activity. A. Henneman's size principle [28]. B. self-sustained oscillations [29]. C. agonist-antagonist coactivation [30]. D. The match between spiking patterns for periodic movements in [31] (Left), and our simulation results (Right), all for low movement speeds, i.e. $\omega < \omega_c$. Bottom Row: Responses to elemental signals. E. Step Movement. Data for healthy individuals [32] and for patients with cerebellar disease [33], F. Short Pulse. Data for healthy individuals [32], and for patients with cerebellar disease [34], G. Periodic Movement. The top row shows data from [32] (Left), and our simulation results for $\omega < \omega_c$ (Right). The bottom row shows data from [4] (Left), and our simulation results for $\omega > \omega_c$ (Right). We see undesirable phenomena in the bottom row, for example, undershoot (red circle), overshoot (orange circle), and skipped cycles (blue circle).

complex models of neural behavior[27]. Fig. 4C shows how during voluntary contraction of a muscle group, agonist and antagonist muscles can both be active with a specific activation pattern (agonist first, then antagonist, and then agonist again at a lower level). This concurrent activation of agonist and antagonist muscles is referred to commonly as coactivation and is captured by our model.

Our SCS model also reproduces movement responses to some elemental reference inputs in both health and cerebellar disease. The model displays discontinuities during slow movements, as shown in Figure 4D. Figs. 4E,F compare model responses to step and pulse inputs to responses of human subjects to the same input types in health [32] and in cerebellar dysfunction [33,34]. The position signals between model and experimental data qualitatively match very well. We model cerebellar degeneration by decreasing the gain parameters of the cerebellar model (K_d, K_p, K_i and I_2) by 60% as well as increasing the muscle stiffness K_m by 4 times, to simulate the typical compensation strategy displayed by patients [15]. Cerebellar patients are known to display dysmetria, specifically hypermetria (or significant overshoot), as well as oscillatory activity past the end of the movement. We see this effect in the model simulations in Figs. 4E,F.

Finally, and most importantly, in Fig. 4G, we show that our SCS model is able to maintain good tracking performance to a sinusoidal input until the input frequency is larger than the fundamental frequency ω_c. After this input frequency, the model displays undesirable phenomena seen in experimental data, including (i) undershoot, (ii) overshoot, and (iii) skipped cycles. Both undershoot and overshoot are phenomena accompanying fast movements in general, i.e., tolerating lower accuracy while reaching for a target, and then correcting the movement when close to the

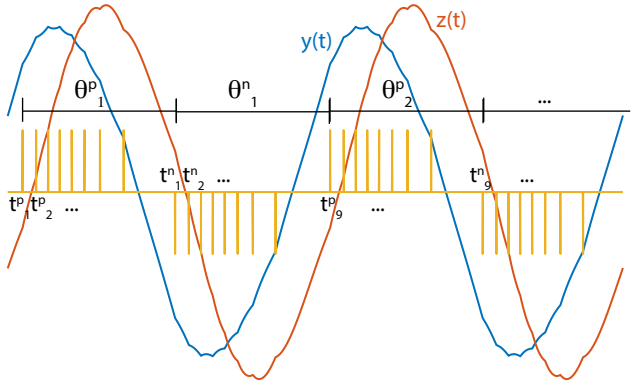

Figure 5: A graphical illustration of positive spike times $\{t_k^p\}_{k\in\mathcal{Z}}$, negative spike times $\{t_k^n\}_{k\in\mathcal{Z}}$, and spike period $\max_{k\in\mathcal{Z}}(\theta_k^p + \theta_k^n)$.

target. In a repetitive movement, however, the movement is not corrected for the duration of more than one cycle, as seen in Fig. 1B.

SCS Model Enables Analytical Derivation of ω_c Skipped cycles is perhaps the most important feature observed while tracking fast sinusoidal inputs, and this phenomena (a) cannot be modeled using linear systems, and (b) cannot be remedied in open loop using a linear system at the output of the movement.

In the Methods section, we derive a fundamental frequency, ω_c, for which skipped cycles are generated when tracking a sinusoidal input whose frequency is higher than ω_c. More importantly, we compute how ω_c depends on our SCS model parameters. To gain an intuition of our approach for deriving ω_c, let's focus on an important limiting parameter, q, which dictates the density of spikes from alpha motor neurons.

Intuitively, we know that skipped cycles are observed as the density of spikes decreases. In order to track the sinusoidal input, the alpha motor neurons must generate a series of positive spikes to track the increasing part of the sinusoidal reference input, which are then followed by a series of negative spikes to track the decreasing part of the sinusoidal reference input. We show that when each spike generated by the positive and the negative IAF, the state of the closed loop SCS model jumps to a new state. Since the output of the SCS is a function of the state, we need the 'spike period', i.e. the maximum length of time between the *sequence* of positive spikes to the *sequence* of negative spikes and back to be higher than the frequency of the sinusoidal input in order to track it at the output.

If the spike period between the series of positive and negative spikes and back is less than or equal to the period of the desired oscillations, then movements are performed without skipped cycles. If the spike period is greater than the period of the desired oscillations, then the output z is not periodic with the same period as the input, and skipped cycles are observed at the output, as shown in Figure 6C. In the Methods section, we derive sufficient conditions for avoiding skipped cycles.

To calculate the minimum switching frequency required to avoid skipped cycles, and its dependence on system parameters, we build a switching map from one spike to the next, and analytically determine the switching times. We can then determine whether the switching frequency between the series of positive and negative spikes is less than the frequency of the driving oscillation for some initial conditions of the system.

Briefly, let the positive and negative spike times be defined as $\{t_i^p\}_{i\in\mathcal{Z}}$ and $\{t_i^n\}_{i\in\mathcal{Z}}$ respectively. Let $\{\theta_k^p\}_{k\in\mathcal{Z}}$ be defined as the time between the first positive spike in a sequence of positive spikes and the first subsequent negative spike, and similarly for $\{\theta_k^n\}_{k\in\mathcal{Z}}$. See Figure 5. Note that for the output z to be periodic with some frequency ω, the input to the musculoskeletal system, i.e. u the spikes, need to be periodic with the same frequency ω. This leads us to the following definition.

Definition 1: Let $r(t) = R\sin(2\pi\omega t + \phi)$, and consider the closed loop system shown in Figure 3, with known initial conditions. We define the presence of **skipped cycles** as the case where the union of the positive and negative spike trains contains less than one positive and one negative spike per period of the input, i.e., $\exists k \in \mathcal{Z}$ s.t. $\theta_k^p + \theta_k^n > \frac{1}{\omega}$.

Conjecture: Let $r(t) = R\sin(2\pi\omega t + \phi)$, and the closed loop system as in Figure 3. There exists an, ω_c, such that for all $\omega > \omega_c$, there exist initial conditions which lead to skipped cycles. Conversely, as q increases, there exist initial conditions which lead to skipped cycles.

In the Methods section, we provide details on the equations pertaining to the conjecture for two specific choices of M, F and K. In particular, we compute ω_c as a function of model components (K, q, M, F) as described in the previous section. Fig. 6 shows the calculated ω_c as a function of q given a specific M, F and K. As expected, as the spiking density increases (q decreases), more information about the cerebrocerebellar output is transmitted to the muscles, i.e. neural computation increases, and we see that the tracking performance increases (ω_c increases).

We also observe that as the feedback gain, F, or as the bandwidth of the musculoskeletal system M increases, we have a larger ω_c for all values of q. Moreover, as the cerebellar proportional gain (K_p) increases, ω_c increases, but not significantly. However, as the cerebellar derivative gain (K_d) increases, ω_c increases drastically, showing the large degree of sensitivity to K_d. The derivative action is hypothesized to take place in the dentate neurons of the cerebellum [15], which are known to be important for rapidly implementing a desired action [35,36]. This feature is corroborated in Fig. 6D.

SCS Model with Compensation Improves Performance for Compromised Neural Activity

The formulation in this paper *quantifies* the increase in maximum speed gained due to the system parameters. It can also help us compensate in limbs by providing either electrical stimulation directly to the muscles, or using an exoskeletal device that can provide extra assistence to the limb. An example of these ideas is presented in Fig. 7. Here, the block for neural activity contains the cerebrocerebellar model as well as the IAF block with the threshold parameter q as earlier. Let ω_c as a function of q for the normal regime be given by the blue curve in Fig. 7B, and let the neural activity be compromised such that q increases (this could correspond to a damage directly in the alpha motor neurons or the spine).

If we add a compensator as in Fig. 7A, which measures the output of the musculoskeletal system, and in turn stimulates the musculoskeletal system in feedback (here, $C = 10$ and thus $M_{new} = \frac{M}{1+MC}$), and the output of the musculoskeletal system is also driven up by the same amount, i.e. $z_{new} = 10z$, then we can drive up the operating curve for ω_c to the red curve shown

in Fig. 7B. This suggests that it in theory one can compensate for damage to the neural system using reinforcements, perhaps via neuroprosthetics, at the musculoskeletal end. Moreover, the framework allows us to quantitatively design compensators, C, given SCS parameters, i.e. K, q, F, and M to meet specific control objectives.

Discussion

Humans can make flexible and fairly fast movements, however damage to various parts of the central nervous system can limit motor performance. Whether damage is caused by stroke, multiple sclerosis, amyotrophic lateral sclerosis, or spinal cord injury, weakness (paresis) occurs routinely after injury to the primary motor cortex (M1) or its output to the spinal cord. This weakness is known to be associated with reduced voluntary recruitment of motor units in the spinal cord, both in terms of the number of motor units recruited and the firing rates they achieve. Given that weakness translates to deficient production of muscular forces that are used to accelerate the limbs, we expect weakness to limit fast movements, with progressively more reduction of neural activity being associated with a deceleration of voluntary movements. However, to the best of our knowledge, this is the first time that a tradeoff between neural computing and motor tracking accuracy have been quantified.

Our modeling framework provides us with an explicit dependence of the emergence of undesirable phenomena (skipped cycles) as a function of q, the parameter that directly dictates the density of spikes (neural computing), the musculoskeletal system M, and cerebrocerebellar dy-

namics K. Specifically, we show that for a fixed musculoskeletal system M, cerebrocerebellar dynamics K, and a pair of motor neurons with thresholds q (for activation of agonist/antagonist pair of muscles), the oscillation input (periodic back-and-forth movement) with frequency ω may generate undesired skipped cycles if ω is 'too large' and/or the density of spikes (related to q) is 'too small'. Such undesirable phenomena are consistent with symptoms observed in patients with movement disorders, and finger tracking experiments wherein subjects are trained to follow a trace back and forth quickly.

A critical component in our SCS model that captures undesirable tracking phenomena in the fast regime is the pulsatile control implemented by alpha motor neurons. Pulsatile constrol of movement has provided us with insights in the 'slow' regime, but has rarely been analyzed for limitations in tracking fast movements. Our SCS model can reproduce experimentally known properties of motor neurons and responses to step, pulse and sinusoidal signals. However, other threshold-based pulsatile models for neural control can be readily used in the theoretical framework developed here. Furthermore, multi-joint muscle models can easily be handled by our framework as adding joints simply adds dimensionality to M. Finally, our framework can be augmented to allow incorporation of transmission delays incurred by the spinal cord. Small delays can be approximated by first order linear systems (Pade approximations [37]) while larger delays in feedback interconnections can be modeled as structured uncertainty.

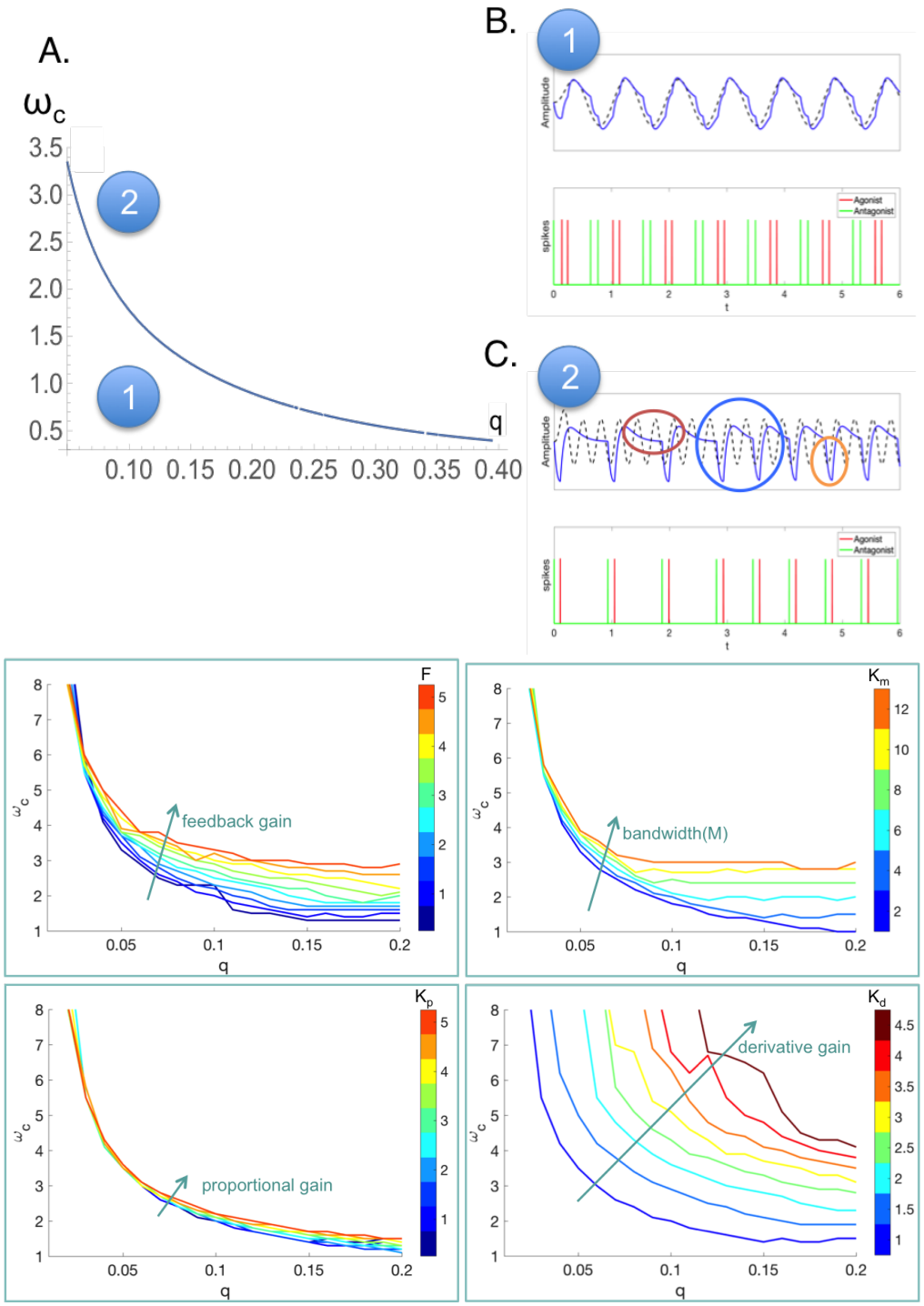

Figure 6: A. ω_c for $R = 1$, $K = 1$, $F = 1$, for varying q. B. $q = 0.1$, $\omega = 1$. C. $q = 0.1$, $\omega = 3.18$. D. ω_c as a function of feedback gain F. E. ω_c as a function of muscle stiffness K_M. F. ω_c as a function of cerebellar proportional gain K_p. G. ω_c as a function of cerebellar derivative gain K_d.

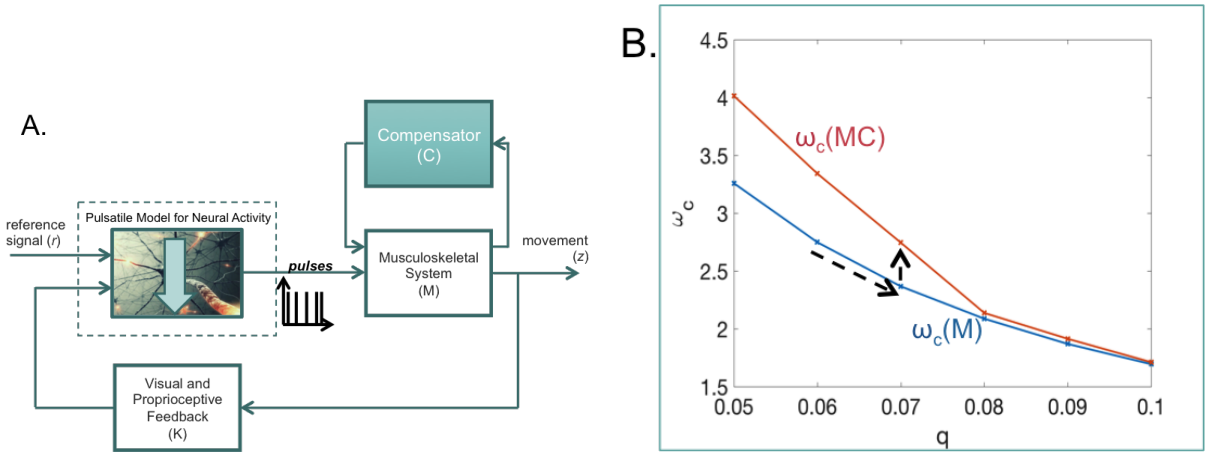

Figure 7: Design of a compensator to restore functioning of the SCS in the presence of a compromised neural system; more details in the text.

Methods

We analytically study the case where the neural activity driving the muscle can be modeled by IAF models. IAF models have been used to model motor neurons in both experimental and computational studies [24,25]. Each IAF system integrates the input signal till the integral reaches a threshold q, at which time it produces a weighted spike $q\delta(t)$, as shown in Fig. 3B. These spikes innervate the corresponding agonist and antagonist muscle models, as shown in Fig. 3.

We study the output of the closed-loop system under periodic forcing, specifically $r(t) = R\sin(2\pi\omega t + \phi)$, and we are interested in how well $z(t)$ follows $r(t)$ as the frequency of the reference movement signal ω increases. Note that for the output z to be periodic with the same frequency ω, the input to the musculoskeletal system, i.e. u the spikes, need to be periodic with the same frequency ω. If all the components of the feedback system were linear, this periodic signal

at that frequency would be present in the output signal, albeit with an amplitude and phase that depends on the gain of the individual systems. However, the specific nonlinearity acts in such a way as to not transmit information if the amplitude of the integral of the signal y falls between $-q$ and q. This inherently ties together the amplitude of the integral of y and the frequency of the desired movement r, and leads to the conditions laid down below for the feedback system to reliably transmit the periodic signal.

We show the conditions for skipped cycles here for a simple case, where $K = 1$, $M = \frac{1}{s+a}$, and $F = 1$, for some $a > 0$, i.e. $A_M = -a$, $B_M = 1$, $C_M = 1$, $D_M = 0$. We first describe the dynamics of $z(t)$ for any t between two spikes t_k and t_{k+1}, i.e. $t_k \leq t < t_{k+1}$ as the following. Specifically, $\{t_k\}_{k\in\mathcal{Z}} = \cup\left(\{t_i^p\}_{i\in\mathcal{Z}}, \{t_i^n\}_{i\in\mathcal{Z}}\right)$.

$$
\begin{aligned}
u(t) &= \sum_{i=0}^{k} q_i \delta(t - t_i) && (5)\\
z(t) &= \mathrm{e}^{-at} z(0) + \int_0^t \mathrm{e}^{-a(t-\tau)} y(\tau) d\tau && (6)\\
&= \mathrm{e}^{-at} z(0) + \sum_{i=1}^{k} q_i \mathrm{e}^{-a(t-t_i)} && (7)\\
&= \mathrm{e}^{-at} z(0) + \mathrm{e}^{-at} \sum_{i=1}^{k} q_i \mathrm{e}^{at_i} && (8)\\
&\equiv \mathrm{e}^{-at} A_k && (9)
\end{aligned}
$$

Here, $A_k \equiv \sum_{i=1}^{k} q_i \mathrm{e}^{at_i} + A_0$, where $A_0 = z(0)$, and we assume that $t_0 = 0$.

At all times, $y(t) = z(t) - r(t)$, and the value of $q_k = \int_{t_k}^{t_{k+1}} y(\tau) d\tau$. Thus, given a sequence

of $\{q_k\}_{k\in\mathcal{Z}}$, where $q_k \in \{q, -q\}$, we have the following condition for the dynamics.

$$\begin{aligned} q_k &= \int_{t_k}^{t_{k+1}} r(\tau)d\tau - \int_{t_k}^{t_{k+1}} z(\tau)d\tau \\ &= \int_{t_k}^{t_{k+1}} R\sin(2\pi\omega\tau+\phi)d\tau - A_k\int_{t_k}^{t_{k+1}} \mathrm{e}^{-a\tau}d\tau \\ &= \frac{R}{2\pi\omega}\left(\cos(2\pi\omega t_k+\phi) - \cos(2\pi\omega t_{k+1}+\phi)\right) + \frac{A_k}{a}\left(\mathrm{e}^{-at_{k+1}} - \mathrm{e}^{-at_k}\right) \end{aligned}$$

The system can be entirely described by the state A_k and time of switching t_k. The switching map $\mathbf{\Pi}$ given a sequence of $q's$, i.e. $\{\pm q, \pm q, \ldots\}$ for the state and spike times is as below.

$$\ldots \xrightarrow{\Pi_{k-1}} \begin{bmatrix} A_k \\ t_k \end{bmatrix} \xrightarrow{\Pi_k} \begin{bmatrix} A_{k+1} \\ t_{k+1} \end{bmatrix} \xrightarrow{\Pi_{k+1}} \begin{bmatrix} A_{k+2} \\ t_{k+2} \end{bmatrix} \xrightarrow{\Pi_{k+2}} \ldots \tag{10}$$

, where A_{k+1} and t_{k+1} are such that:

$$A_{k+1} = A_k + q_{k+1}\mathrm{e}^{at_{k+1}} \tag{11}$$

$$\frac{R}{2\pi\omega}\cos(2\pi\omega t_{k+1}+\phi) - \frac{A_k}{a}\mathrm{e}^{-at_{k+1}} = -q_k + \frac{R}{2\pi\omega}\cos(2\pi\omega t_k+\phi) - \frac{A_k}{a}\mathrm{e}^{-at_k} \tag{12}$$

In general, this system can have multiple positive spikes in a row and multiple negative spikes in a row. We define θ_k^p and θ_k^n recursively as the following (see also Figure 5).

$$\theta_1^p = t_1^n - t_1^p \tag{13}$$

$$\theta_1^n = \min_{j\in\mathcal{Z}}\left(t_j^p - t_1^n\right) \tag{14}$$

$$\theta_k^n = \min_{j\in\mathcal{Z}}\left(t_j^p - \left(\sum_{i=1}^{k-1}\theta_{k-1}^p + \theta_{k-1}^n + \theta_k^p + t_1^p\right)\right) \tag{15}$$

$$\theta_k^p = \min_{j\in\mathcal{Z}}\left(t_j^n - \left(\sum_{i=1}^{k-1}\theta_{k-1}^p + \theta_{k-1}^n + t_1^p\right)\right) \tag{16}$$

Note that for the spike train to be periodic with at least frequency ω, $\max_k(\theta_k^p + \theta_k^n) > \frac{1}{\omega}$. If the condition $\max_k(\theta_k^p + \theta_k^n) > \frac{1}{\omega}$ is not met, we have skipped cycles at the output z. Thus, we can find the dependence of $\max_k(\theta_k^p + \theta_k^n)$ on q for a given system with a given sinusoidal reference signal r.

Due to the transcendental nature of Equations 11 and 12, a numerical solution is required. This is obtained by forward marching in time using a suitably chosen time step, for each set of initial conditions $z(0)$ and ϕ. We perform the numerical solution for 20 different randomly chosen values of $z(0)$ and 12 different values of ϕ, and take the maximum $(\max_{k,z(0),\phi}(\theta_k^p + \theta_k^n))$ of these, hereafter written as $(\max_k(\theta_k^p + \theta_k^n))$ for short. In Figure 8, we show $\omega \max_k(\theta_k^p + \theta_k^n)$ as a function of q for several values of ω for two sets of specific system parameters; one for $K = 1$, $M = \frac{1}{s+1}$, and $F = 1$, and the second for $K = 1$, $M = \frac{K_m}{I_m s^2 + B_m s + K_m}$, with $K_m = 1,\ I_m = 1,\ B_m = 1$, $R = 1$ and several values of ω. We see that for both cases, as we increase q, we hit the regime termed the undesirable regime, namely with skipped cycles, with $\omega(\max_k(\theta_k^p + \theta_k^n)) > 1$. Thus, we show the conjecture detailed in the Results section for specific systems.

More details for general K and M, as well as approximation methods for determining ω_c, are discussed in [38].

Correspondence Correspondence and requests for materials should be addressed to S.S. (email: ss5513@columbia.edu).

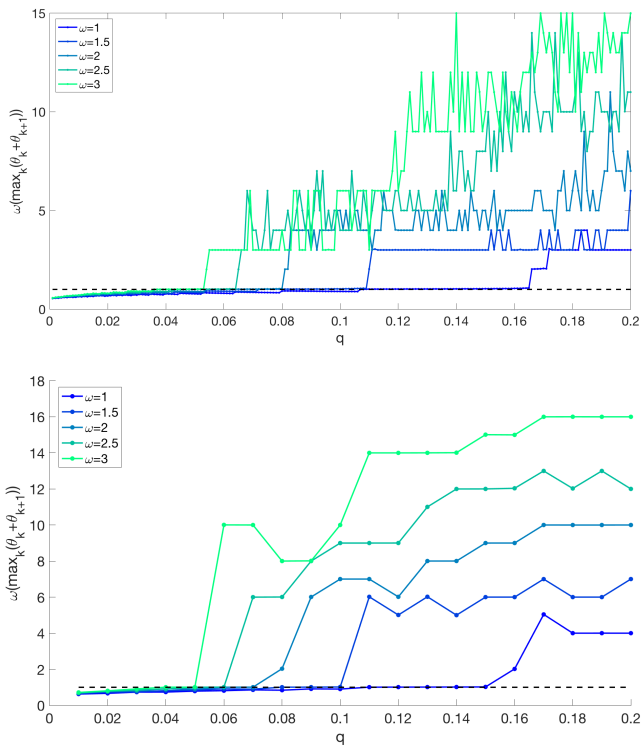

Figure 8: $\omega(\max_k(\theta_k^p + \theta_k^n))$, for several values of ω and q, for two different systems. If this is greater than 1, the system displays skipped cycles. Top: $K = 1$, $M = \frac{1}{s+1}$, $F = 1$. Bottom: $K = 1$, $M = \frac{K_m}{I_m s^2 + B_m s + K_m}$, with $K_m = 1,\ I_m = 1,\ B_m = 1$. The systems were solved forward in time for multiple values of initial conditions $z(0)$ and ϕ.

1. Hanneton, S., Berthoz, a., Droulez, J. & Slotine, J. J. Does the brain use sliding variables for the control of movements? *Biological cybernetics* **77**, 381–393 (1997).

2. Schmid, R. & Ron, S. A model of eye tracking of periodic square wave target motion. *Biological Cybernetics* **54**, 179–187 (1986).

3. Fuchs, A. Periodic eye tracking in the monkey. *The Journal of physiology* **193**, 161 (1967).

4. Vince, M. A. Corrective movements in a pursuit task. *Quarterly Journal of Experimental Psychology* **1**, 85–103 (1948).

5. Fitzpatrick, R., Burke, D. & Gandevia, S. C. Loop gain of reflexes controlling human standing measured with the use of postural and vestibular disturbances. *Journal of neurophysiology* **76**, 3994–4008 (1996).

6. Craik, K. J. Theory of the human operator in control systems. *British journal of psychology* **38**, 56–61 (1947).

7. Fishbach, A., Roy, S. A., Bastianen, C., Miller, L. E. & Houk, J. C. Deciding when and how to correct a movement: Discrete submovements as a decision making process. *Experimental Brain Research* **177**, 45–63 (2007).

8. Loram, I. D., Gollee, H., Lakie, M. & Gawthrop, P. J. Human control of an inverted pendulum: is continuous control necessary? Is intermittent control effective? Is intermittent control physiological? *The Journal of Physiology* **589**, 307–324 (2011).

9. Loram, I. D., Van De Kamp, C., Lakie, M., Gollee, H. & Gawthrop, P. J. Does the motor system need intermittent control? *Exercise and Sport Sciences Reviews* **42**, 117–125 (2014).

10. Miall, R. C., Weir, D. J. & Stein, J. F. Intermittency in human manual tracking tasks. *Journal of Motor Behavior* **25**, 53–63 (1993).

11. Novak, K., Miller, L. & Houk, J. The use of overlapping submovements in the control of rapid hand movements. *Experimental Brain Research* **144**, 351–364 (2002).

12. Wolpert, D. M., Miall, R. C., Winter, J. L. & Stein, J. F. Evidence for an Error Deadzone in Compensatory Tracking. *Journal of Motor Behavior* **24**, 299 (1992).

13. Farmer, S. F. Pulsatile central nervous control of human movement. *J.Physiol.* **517**, 3 (1999).

14. Jo, S. & Massaquoi, S. G. A model of cerebrocerebello-spinomuscular interaction in the sagittal control of human walking. *Biological Cybernetics* **96**, 279–307 (2007).

15. Jo, S. & Massaquoi, S. G. A model of cerebellum stabilized and scheduled hybrid long-loop control of upright balance. *Biological cybernetics* **91**, 188–202 (2004).

16. Massaquoi, S. G. & Topka, H. Models of cerebellar function. *The cerebellum and its disorders. Cambridge University Press, Cambridge* 69–94 (2002).

17. Kandel, E. R., Schwartz, J. H., Jessell, T. M. *et al.* *Principles of neural science*, vol. 4 (McGraw-Hill New York, 2000).

18. McIntyre, J. & Bizzi, E. Servo hypotheses for the biological control of movement. *Journal of motor behavior* **25**, 193–202 (1993).

19. Todorov, E. & Jordan, M. I. Optimal feedback control as a theory of motor coordination. *Nature neuroscience* **5**, 1226–1235 (2002).

20. Shadmehr, R., Smith, M. A. & Krakauer, J. W. Error correction, sensory prediction, and adaptation in motor control. *Annual review of neuroscience* **33**, 89–108 (2010).

21. Wolpert, D. M., Ghahramani, Z. & Jordan, M. I. An internal model for sensorimotor integration. *Science-AAAS-Weekly Paper Edition* **269**, 1880–1882 (1995).

22. Laughlin, S. B., de Ruyter van Steveninck, R. R. & Anderson, J. C. The metabolic cost of neural information. *Nature neuroscience* **1** (1998).

23. Watson, C., Kirkcaldie, M. & Paxinos, G. *The brain: an introduction to functional neuroanatomy* (Academic Press, 2010).

24. Goroso, D., Cisi, R. & Kohn, A. The amplitude and phase responses of the firing rates of some motoneuron models. *Biosystems* **58**, 33–39 (2000).

25. Cofer, D. *et al.* Animatlab: a 3d graphics environment for neuromechanical simulations. *Journal of neuroscience methods* **187**, 280–288 (2010).

26. Henneman, E. & Mendell, L. Functional organization of motoneuron pool and its inputs. *Handbook of physiology* 423–507 (1981).

27. Henneman, E. & Mendell, L. M. Functional organization of motoneuron pool and its inputs. *Comprehensive Physiology* (2011).

28. Henneman, E., Somjen, G. & Carpenter, D. O. Excitability and inhibitibility of motoneurons of different sizes. *Journal of neurophysiology* **28**, 599–620 (1965).

29. Heckman, C., Johnson, M., Mottram, C. & Schuster, J. Persistent inward currents in spinal motoneurons and their influence on human motoneuron firing patterns. *The Neuroscientist* (2008).

30. Ghez, C. Muscles: effectors of the motor systems. *Principles of neural science* 548–563 (1991).

31. Joachim Büdingen, H. & Freund, H.-J. The relationship between the rate of rise of isometric tension and motor unit recruitment in a human forearm muscle. *Pflügers Archiv European Journal of Physiology* **362**, 61–67 (1976).

32. Navas, F. & Stark, L. Sampling or intermittency in hand control system dynamics. *Biophysical Journal* **8**, 252–302 (1968).

33. Manto, M. Mechanisms of human cerebellar dysmetria: experimental evidence and current conceptual bases. *Journal of neuroengineering and rehabilitation* **6**, 10 (2009).

34. Hore, J. & Vilis, T. A cerebellar-dependent efference copy mechanism for generating appropriate muscle responses to limb perturbations. In *Cerebellar functions*, 24–35 (Springer, 1984).

35. Pruszynski, J. A. & Scott, S. H. Optimal feedback control and the long-latency stretch response. *Experimental brain research* **218**, 341–359 (2012).

36. Thach, W., Perry, J., Kane, S. & Goodkin, H. Cerebellar nuclei: rapid alternating movement, motor somatotopy, and a mechanism for the control of muscle synergy. *Revue neurologique* **149**, 607–628 (1992).

37. Aström, K. J. & Murray, R. M. *Feedback systems: an introduction for scientists and engineers* (Princeton university press, 2010).

38. Saxena, S. *Moving fast: neural constraints in closed loop*. Ph.D. thesis, Massachusetts Institute of Technology (2017).